Development and optimization analysis of cryogenic automatic sample changer for neutron scattering at CSNS*

Ji-Xin Chen,[1,2,†] Bo Bai,[1,3,4,†] Fa-Liang Cheng,[2] Yuan Sun,[1,3,4] Hui Cheng,[1,3,4] Bao Yuan,[1,3,4] Meng-Jia Dou,[1,3,4] Chen-Yang Wang,[1,3,4] Quan Lin,[1,4] Zi-Cong Lu,[1,4] Lin-Jin Deng,[1,2,4] Xin Tong,[1,3,4,‡] and Hai-Tao Hu[1,3,4,§]

[1]*Spallation Neutron Source Science Center, Dongguan 523803, China*
[2]*Dongguan University of Technology, Dongguan 523808, China*
[3]*Institute of High Energy Physics, Chinese Academy of Sciences, Beijing 100049, China*
[4]*Guangdong Provincial Key Laboratory of Extreme Conditions, Dongguan, 523803, China*

The use of automatic sample exchange technology can greatly improve the efficiency of neutron scattering experiments. China spallation neutron source (CSNS) has currently developed a cryogenic sample changer that design for exchange sample in the temperature range of 100K to 300K and finally achieve the minimum operating temperature is 80K. Samples are provided with a temperature ranging from 4.2K to 800K by CCR-02 through a closed cycle refrigerator (CCR) and a heater. This paper introduces the structure of the sample changer, which can accommodate up to 24 samples and the replacement time of each sample does not exceed 2 minutes. CSNS II phase will develop a second generation sample changer with an operating temperature range from 10K to 350K. For this requirement, we researched why the chain drive jammed in 80K and redesigned the chain and the support. By simulating in Ansys Workbench, we concluded that the new chain has more excellent performance in low-temperature and its stress is small and uniform. Because of the stress concentration, the S chain plate with a clamping angle of 20° is selected. The new support under Fluent can get the lowest temperature is 4.48K (316 stainless steel) and 4.23K (titanium). The new design will be tested after processing is completed.

Keywords: cryogenic, automatic sample change, mechanical design, simulation

I. INTRODUCTION

China Spallation Neutron Source (CSNS) is a major scientific and technological infrastructure and a large-scale research platform for multidisciplinary applications [1–3]. The first phase of the project passed the engineering acceptance organized in August 2018 and was officially opened for operation to users. The proton beam power reached a power of 160 kW in March 2024 [4, 5]. The construction of CSNS Phase II officially started in January 2024. As of February 2024, CSNS has completed 11 rounds of open operation, and the demand for beam time exceeds the supply. The neutron beamlines, including the General Purpose Powder Diffractometer, the Multi-functional Reflectometer, the Small Angle Neutron Scattering Instrument, and the Multi-physics instrument. In addition, there are 14 other spectrometers under construction that will be accessible to the public in the near future. CSNS had completed over 1300 research projects [6–9]. Significant scientific achievements have been made in the fields of lithium-ion batteries, solar cell structures, rare earth magnetism, new high-temperature superconductors, quantum materials, functional films, high-strength alloys, and chip single-particle effects. It will provide an advanced and powerful scientific research platform for China's materials science and technology, physics, chemistry and chemical engineering, life science, resources and environment, and new energy [10–14].

Neutron scattering experiments need to be carried out in different sample environments. These sample environments usually include vacuum, low temperature, high temperature, magnetic field, etc. Different sample environments will be utilized when the experiment requires a specific sample condition [15–17]. During the construction phase of the CSNS project, three types of equipment for variable sample temperature environments were designed and manufactured [18, 19]. The variable temperature sample environment mainly adopts different adjustment methods such as low temperature refrigeration, heating and constant temperature to provide more precise temperature control for studying different systems. Three types of sample temperature variable environment equipment were designed and manufactured during the construction of the first phase of CSNS project, including cryostats in the low-temperature zone, water bath cryostats in the medium-temperature zone, and neutron scattering high-temperature furnaces in the high-temperature zone. They works at temperature range from 0.3 K to 300 K, 243 K to 473 K and 473 K to 2 073 K respectively. In biochemistry, variable temperature sample environments can be used to study protein structure and function [20]. In materials science, variable temperature sample environments can be used to study material properties such as phase change, thermal

* supported by the National key R&D program of China (No. 2022YFA1604104)
Youth Innovation Promotion Association CAS, the National Natural Science Foundation of China (Grant No. U2230207)
the ninth batch of innovation and entrepreneurship leading talents (innovation category) in 2019, Guangdong Natural Science Funds for Distinguished Young Scholar (No. 2021B1515020101)
Guangdong Provincial Key Laboratory of Extreme Conditions, Guangdong Basic and Applied Basic Research Foundation (No. 2023A1515011797), and the China Postdoctoral Science Foundation (2023M742045). Guangdong Provincial Key Laboratory of Extreme Conditions (2023B1212010002).
† The first author and the second author contribute equally to this work
‡ Corresponding author, tongx@ihep.ac.cn
§ Corresponding author, huht@ihep.ac.cn

expansion coefficient, thermal conductivity, etc [21, 22]. The majority of neutron scattering experiments are conducted in low-temperature sample environments. This is because low temperatures effectively reduce the thermal motion of atoms, thereby improving experimental precision and providing a platform for research on low-temperature phase transitions and superconductivity [23–27].

The samples need to be changed manually after each neutron scattering experiment when an automatic sample changer is not available. This process requires turning off the neutron beam and wastes of precious beam time. Then installing a new sample, this step will expose operators to radiation and increases their exposure time. The process of install the sample will produce unavoidable human errors each time. Therefore, the major spallation neutron sources in the world had development of low-temperature automatic sample exchange technology.

The POWGEN automatic changer (PAC) is utilized on the powder diffraction spectrometer at the Oak Ridge National Laboratory. The PAC has gone through three generations of development. The samples are cooled by the closed cycle refrigerator or heated by the heater. This set of equipment can realize the automatic replacement of 24 samples. The refrigeration time and replacement time of samples for each generation of PAC are different from each other. The sample changers of all three generations have achieved the rapid replacement of samples. This has greatly improved the efficiency and reliability of the experiment [28–30]. The nanoscale ordered material diffractometer is equipped with the automatic sample changer that can operate in the temperature range of 90K-500K [31].

ISIS has also developed automatic sample exchange technology, such as the Iris Three Position Sample Changer which can accommodate three sample cans that size up to 40mm$\times$40mm in the vertical direction. Automatic sample exchange is achieved by means of vertical movement. Furthermore, it has a minimum operating temperature of 4.2 K[32]. The Parachute Sample Changer used an industrial robot to exchange samples which sample cans up to 40 mm in length and 6.4 mm in diameter. The sample can is assembled a baffle. The shape of baffle is like a parachute, which ensure that the sample can captures exchange gas and stably move. This cryogenic automatic sample changer uses two very interesting technologies. One is the use of gas transport technique, and the other is the separation of the cryogenic environment and the motion system. Movement through the CCR is controlled by the flow of exchange gas underneath the sample position. The baffle impedes the gas flow creating a pressure, forcing the can out of the CCR [33, 34].

The BL-21 automatic sample changer at the J-PARC can automatically exchange 18 samples in the temperature range from 20K to 500K [35].

CSNS has developed automatic sample exchange technology too. The Small Angle Neutron Scattering Instrument developed two sample changers. The one of them can exchange 36 samples in the temperature range of -30°C to 300°C [36]. The other one can operate at 10K and its maximum change number of samples are four [37]. CSNS also has developed an automatic sample changer that can operate in the temperature range from 100K-300K. The maximum auto exchange number of samples are 24 in this sample changer. Its transmission system can move the sample at a speed of 1mm/s to 5mm/s. This sample changer takes less than 2 minutes to complete transmission of a sample to experiment position. Excluding the waiting time for the experiment, the time to complete the automatic exchange of a batch of samples is less than 45 minutes. Additionally, The sample can be seen through the glass window. In this automatic sample changer, O-rings are used for sealing in order to achieve better sealing performance. The clamp is used to connect the automatic sample changer and the cryostat. The cryostat is the CCR-02 of CSNS, which can provide the experiment temperature range from 4.2K to 800K.

In summary, automatic cryogenic sample exchange technology is crucial for neutron scattering experiments. It not only improves the experimental efficiency, but also maximizes the use of precious neutron beam. The changer which mentioned in the paper is directly inserted into the sample chamber of the cryostat. This method can save space. Our goal is to achieve lower temperatures and to exchange a more number of samples.

This paper describes the principle and structure of the automatic sample changer. For the requirements of CSNS Phase II, the structure of the sample changer was optimized so that it can work under lower temperature conditions. In this paper, the design of an “S” type chain (hereinafter referred to as S chain) and the support skeleton has a hollow design will be introduced in detail. By analyzed the simulation results, the conclusions shows that S chain has more excellent performance such as less stress and less offset than ordinary chain. The Fluent is utilized to calculate the lowest temperature that the new design can achieve.

II. THE DESIGN AND EXPERIMENT

Conventional cryostats can be divided into wet storage cryostats, continuous flow cryostats and cryostats with refrigerators according to their working principles. Wet storage cryostat exhibit excellent temperature gradient and stability, but to obtain lower temperature, it needs to consume more liquid helium. The temperature control is easy to achieve. The cryostat with a refrigerator consumes a small amount of helium when samples are changed manually. Based on sample placement methodology, cryostats with refrigerators are divided into direct-cooling cryostats and non-direct-cooling cryostats. The direct cooling type places the sample in direct contact with the cold head of the refrigerator. Although changing the sample is more cumbersome, the cooling speed is fast and the lowest temperature can reach below 4.2 K. The non-direct cooling sample does not come into direct contact with the cold head. The sample is placed in the exchange gas with uniform temperature. The refrigerator does not need to be shut down when changing samples, which makes sample changing convenient. Therefore, this structure is used in most large optical radiation devices, and its lowest temperature can

reach below 1.5 K [38–41].

The whole set of equipment is mainly composed of three parts, cryostat, automatic sample changing plug-in and control part [42]. The design sketch as shown in Fig. 1.

The CCR-02 system is integrated by the main body of the cryostat, a helium tank, a water chiller, a helium compressor, a GM refrigerator, a temperature controller and a vacuum pump. The pump is used to evacuate the vacuum chamber and the sample chamber to vacuum. The sample chamber is filled with 50 kPa helium as the thermal transfer medium. The helium compressor supplies high-pressure helium to the refrigerator, which can create the lowest temperature environment of 4.2 K through the throttling expansion of high-pressure helium. The utilization of a water chiller becomes necessary in order to provide cooling water, which effectively eliminates heat generated by the helium compressor during the compression process. The CCR-02 can achieve a variable temperature range from 4.2 to 800K, which provides a variety of temperature conditions for neutron scattering experiments. Both the vacuum chamber and the heat shield are used to reduce heat transfer with the ambient temperature. The cold head and the heater exchange heat with the helium gas. Accurate temperature control can be achieved by controlling the power of the heater.

The cryogenic sample changer uses a gear drive and a chain drive to realize the transmission function. The sample cans are hung between two chains and be moved together with the chain. The cryogenic sample changer will be described in detail later. The reasons why the chain driver is selected instead of other transmission modes are that the chain driver can better adapt to the needs of equipment layout, it saves space, it is convenient for making a compact connection with the surrounding complex structure, and it has a low maintenance cost. Due to the changer operates in the vacuum, lubricating oil cannot be used for lubrication. Ceramic bearings with good self-lubricating properties are used in this unit.

The control system is divided into two parts: temperature control and motion control. Firstly, the temperature sensor sends the temperature signal to the temperature controller, which regulates the heater's power to achieve precise temperature control. The temperature curve of the entire experimental process is stored and accessed through the computer. Secondly, the moving control system consists of PLC, servo motor and fiber optic sensor. The servo motor and fiber optic sensor are installed on the sample changer of upper bracket. The control process of the control system is as follows: (a) The PLC sends a signal to activate the servo motor; (b) The laser from the fiber sensor is interrupted by the sleeve and another signal is sent to the PLC; (c) the servo sends feedback to the PLC for real-time position monitoring of the sample; (d) the signal from the fiber sensor is used to prevent the motor from stalling; (e) the PLC sends a signal to stop the operation. This method can effectively confirm the position of the samples and whether the device is operating normally.

A. The structure of sample changer

The cryogenic automatic sample changer consists of three primary components: a skeleton, a transmission system, and sample cans. The sample can is entirely made of 6061 aluminum alloy and used to contain different samples such as liquid and powder. The sample cap and tube are threaded together and sealed with indium wire. The cap has a hook for hanging on the sample rod. This rod serves as both a chain pin and a support for the sample can. As shown in Fig. 2(a).

The support skeleton consists of an upper and a lower bracket. The upper bracket is connected to two transmissive fiber optic sensors and one of them is spare. The laser from the fiber optic will be blocked by the the chain sleeve when the chain moving and triggers a signal. Each time the laser from the sensor is interrupted, it indicates that the sample has moved 6.35 mm.(length of chain pitch).

The chain shields are mounted on both sides of the lower bracket to organize wiring and stabilize chain movement during transfer. As shown in Fig. 2(a). There is a heater and a temperature sensor installed at bottom of the lower bracket. The temperature sensor can measure the sample temperature, allowing us to control the heater power for temperature control. The heater works together with CCR-02 to achieve temperature control.

The transmission mechanism integrates dual-chain and synchronous gear drive systems with a 1:1 gear ratio. From Fig. 2(a), two gear drives and chain drivers are used to transmit the samples. In this way, the sample rod can be securely installed in the center of two chains. Furthermore, virtual constraints can be employed to enhance the stability of the sample canister's transmission and ensure a more balanced force distribution across all components. The chain drives are working when the gear drives operating and the sample canister following the chain to move. The transmission system will deliver the next sample to the beam position after the completion of the neutron scattering experiment for the previous sample. Finally, all the experiments are quickly completed. This sample changer can realize the automatic replacement of 24 samples. It takes less than two minutes to complete the replacement of one sample, and it doesn't take more than 45 minutes to complete the replacement of all samples.

The servo motors are designed to be externally mounted and therefore only requires positioning during initial installation. After completing the experiment on all samples, only need to detach the transmission system. Experienced workers can quickly locate and install the cryogenic automatic sample changer after installing the new sample can.

The vacuum hood of cryogenic sample changer is connected with CCR-02 via a clamp. Sample temperature is gauged by temperature sensor. All control tasks mentioned above can be achieved by the PLC. The cryogenic auto sample changer was shown in Fig. 2.

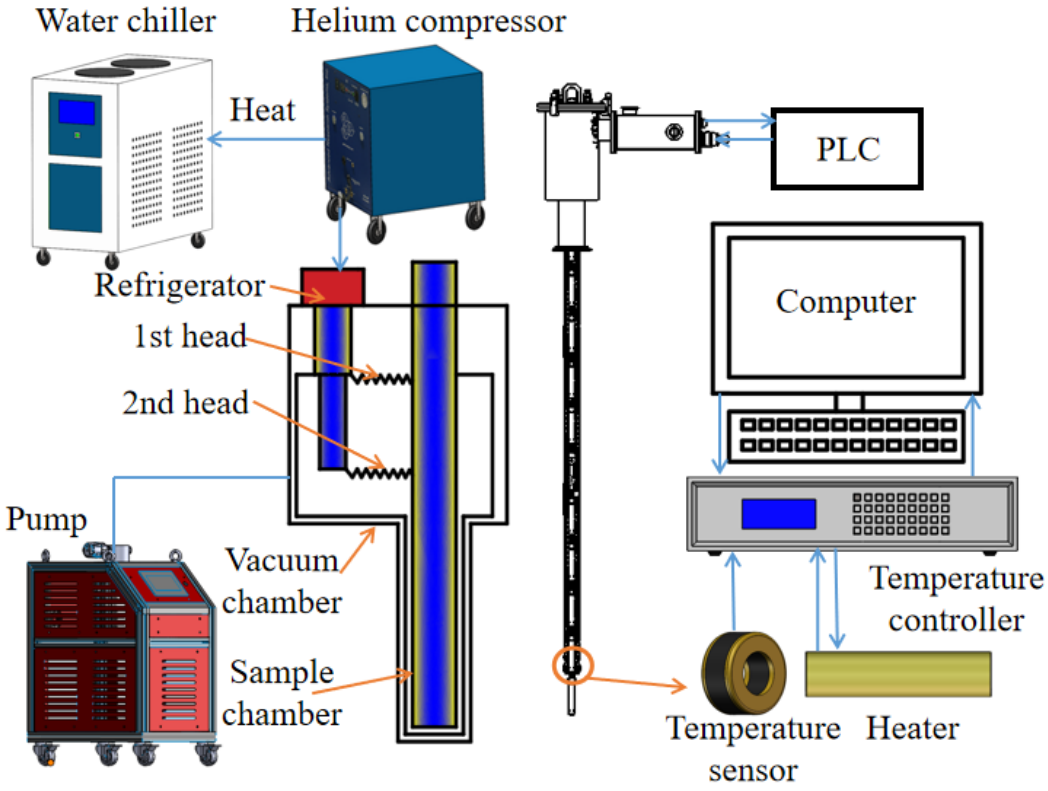

Fig. 1. Schematic diagram of the installation

B. Experiment

The cryogenic sample changer is placed in a support like Fig. 2(b). The experiment platform must be set up before the relevant test. A hoist is employed to lift the sample changer and carefully lower it into the CCR-02 sample chamber, completing the experimental platform setup.

For a reliable experiment condition, leakage detect must be conducted before low temperature test. After connecting to the leak detector, helium gas is used to blow the possible leak point. If the blow point is leakage, the helium will be inhaled to detector and be detected. The device can reach a vacuum degree of $10^{-4}Pa$ in our tests.

The initial test series demonstrated reliable sample changer operation under both atmospheric and vacuum conditions. These results confirmed system readiness for subsequent cryogenic performance evaluation.

1. The cold down experiment with the changer

Since this sample changer is designed to achieve automatic sample change from 100K to 300K. Therefore, the heating experiment didn't be conducted on it. The heater is used when the samples need to heat from low temperature to high temperature. CCR-02 generally takes 5 hours to cool itself and the sample from room temperature to 4.2K. In the cooling test of this sample changer, it took nearly 6.6 hours to drop to the lowest temperature 10.83K at the temperature measure position. Since the sealing and cooling performance of the whole device is acceptable, the low temperature test is conducted overnight and it can still maintain the lowest temperature. During the test, the calibration of the sample temperature isn't conducted, and simply used the temperature value at the measure position of the bracket to instead of the sample temperature. In fact, there is a certain temperature difference between the two positions. There are easily to see that the measure point and the sample has certain distance between the two positions. The sample are more near to the second cold head of the CCR-02. So, the temperature of two positions are different. The calibration will address this issue in the future by installing a second temperature sensor inside the sample can. Temperature data from both locations will be recorded and stored. Using polynomial fitting or other analytical methods, the relationship between the bracket base temperature and the actual sample temperature will be established.

Since the lower bracket has a larger heat leakage, it is difficult to cool it down to below 10K. For the convenience of calculation, the lower bracket is simply simplified to a solid rod.

The formula is calculated according to the heat flux density:

$$\Phi = -\lambda A\frac{\Delta T}{l} = -10\times 0.0003753\times\frac{-286}{1}\ W\ = 1.073W \quad (1)$$

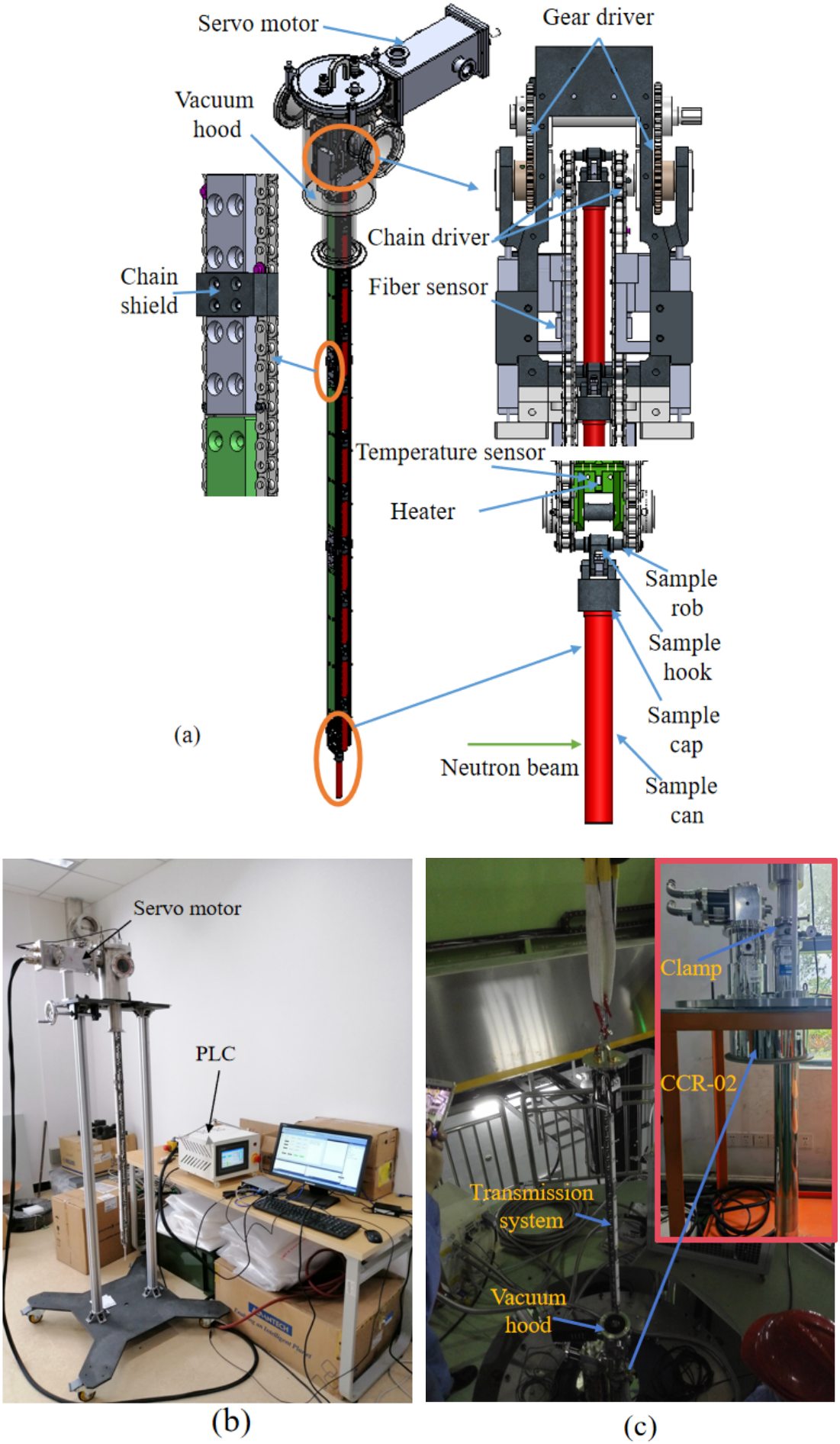

Fig. 2. The sample changer of CSNS. (a) Model of cryogenic automatic sample changer. (b) Sample changer (c) Experiment filed.

The parameters in the equation are: λ is thermal conductivity; A is the cross-sectional area of lower bracket and chain; ΔT is the temperature difference between the bottom and top of the lower bracket; l is the length of lower bracket.

The secondary stage of the CCR-02 cryocooler delivers 1.5W of cooling capacity at 4.2K, while the conductive heat load through the support rod and the chain accounts for nearly two-thirds of this capacity. Equation (1) neglects both radiative heat transfer and parasitic thermal loads from auxiliary components. These unaccounted thermal contributions represent significant heat influxes, constituting the primary limitation in achieving sample temperatures below 10 K. The another factor that affects the cooling effect is the aging of the 2nd head, which reduces its refrigeration efficiency.

For the requirements of CSNS II phase, a new design for the sample changer to get a lower temperature environment. The new design and correcting simulation are shown in section 3.2. The cooling curve is shown in Fig. 3.

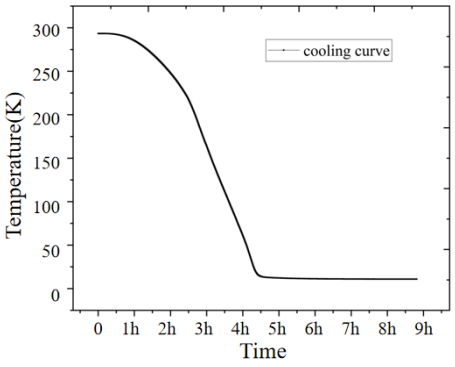

Fig. 3. Colding curve

2. *The lowest working temperature test*

In this experiment, tests are conducted based on temperature changes: when the temperature exceeds 143K, testing occurs after each 10K drop. In the range between 100K and 143K, tests are performed each 5K drop. For temperatures below 100K, testing is carried out for each 1K drop. The test results indicated that the transmission remained stable when the temperature is above 143K. However, when the temperature drops below 143K, the transmission started to jam, and it becomes complete failure at 80K.

The test is conducted to verify the impact of low temperatures on the gear drive. The chain was disassembled and conducted a test in a low-temperature environment. The results indicated that low temperature has no effect on the gear drive system, which operated stably under low temperatures. This indicates that the problem lies within the chain based on the tests conducted above.

The reasons cause of transmission stuck are: with the decrease of temperature, (1) The shrinkage of the chain gradually increases and interactions occur between the chain links; (2) the shrinkage of chain is more than lower bracket and interaction occurs between the chain and bracket; (3) due to the low temperature shaft shrinkage, the chain working position is offset. Above proposed interaction will generate stress and impact the chain drive.

Through the glass window, it can be clearly observed that the inner and outer chain links are offset to both sides, and some chain plates are bent and deformed, as shown in Fig. 4(a). The chain plates occurred plastic deformation after low temperature testing. The computational model of offset is shown in Fig. 4(b) and Fig. 4(c). The chain pitch were not significantly affected by temperature (the influence of calculating the shrinkage of chain pitch is little).

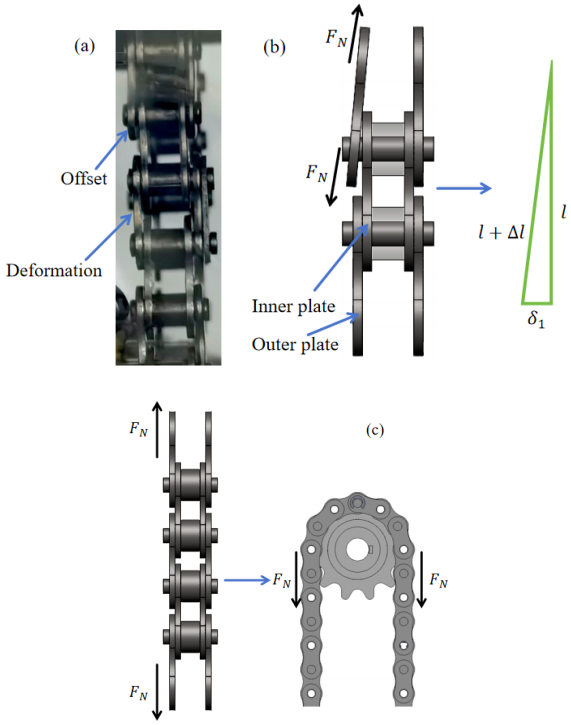

Fig. 4. Offset and the calculating model of chain. (a) Chain transmit from low temperature. (b) Schematic view of chain plate offset. (c) Schematic view of force.

According to Pythagorean theorem, the strain of outer plate:

$$\sqrt{6.35^2 + \delta_1^2} - 6.35 \tag{2}$$

According to Hooke's law:

$$\frac{\Delta l}{l} = \frac{1}{E} \cdot \frac{F_N}{A} \tag{3}$$

So, the extra torque of chain drive:

$$T = \mu F_N \frac{d}{2} = \mu E A \frac{\Delta l}{l} \frac{d}{2} \tag{4}$$

The parameters in the formula: $\triangle l$ is the strain of outer plate; δ_1 is the offset of chain plate; l is chain pitch; E is elastic modulus of 304; F_N is the tensile force from deformation; A is the cross sectional area of chain plate; μ is the friction coefficient; d is the indexing circle of sprocket; T is the extra torque. Some parameters are shown in TABLE 1 and the calculate result is shown in Fig. 5. According to Newton's third law, the action force is equal to the reaction force, so eventually the force will act on the entire chain.

TABLE 1. Calculating parameters

	μ	E	A	d
value	0.3	195GPa	$4.1mm^2$	24.53mm

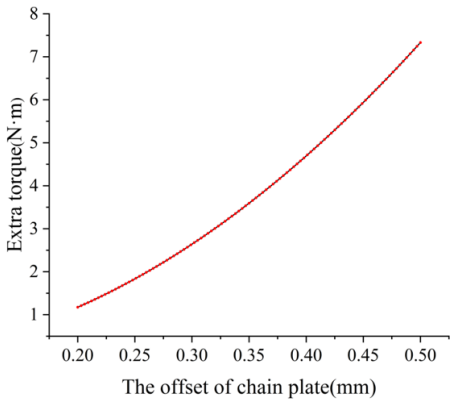

Fig. 5. Extra torque

The analysis determined that the chain drive can operate normally when the offset is less than 0.22mm (rated torque of the motor is $1.29N \cdot m$). However, as the additional torque increases, the chain drive will gradually jam, and when the additional torque is largely enough to trigger the motor's protection program, the transmission will stuck completely.

III. OPTIMIZATION AND ANALYSIS

Through this analysis, the root causes of the chain drive failure have been identified. The optimization in the structure of chain and skeleton for more excellent performance is conducted and has great value.

A. S chain

We are dedicating the majority of our time to researching and designing the S chain, as it is the most crucial component of the changer.

1. *The structure of S chain*

Ordinary chains are composed of inner and outer plates, pins, sleeves, and rollers. Due to the large number of parts, there are more complex stress interactions between various components at low temperatures.

In terms of the structure of chain drive, the S-type chain is different from the ordinary chain. It only consists of chain plates, pins and rollers. Each chain plate contains two holes: a smaller one for interference fitting with the pin and a larger one for clearance fitting (show in Fig. 6(a)).

In order to avoid the chain plate and the pin from affecting each other when they shrink at low temperatures, the interference fit should be calculated during design. The assumption of maximum displacement is made for the chain plate: (1) There is a fixed support at the distal end of adjacent links. (2) The shrinkage of the chain plate only occurs towards the fixed support. The assumption is shown in Fig. 6(b). In this hypothesis, the contraction is only towards both ends of the link. The maximum shrinkage of each chain plates is calculated from the thermal expansion formula:

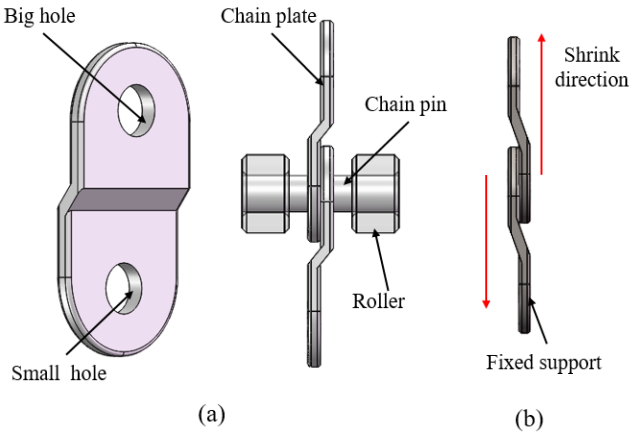

Fig. 6. S chain and assumption. (a) Model of S chain; (b) Assumption of maximum displacement.

$$\Delta\delta_2 = P_1 \Delta T \alpha \tag{5}$$

According to the maximum displacement model, the minimum clearance between the pin and the large hole is $2\triangle\delta_2$. To ensure sufficient clearance at low temperatures, the safety factor K=1.5 is required. The fit clearance of the plate with pin is:

$$X = 2K\Delta\delta_2 = 3P_1\Delta T\alpha \tag{6}$$

The tolerances and fits:

$$X_{Max} = ES - ei \tag{7}$$

$$X_{Min} = EI - es \tag{8}$$

The parameters in the formula: $\triangle\delta_2$ is the shrinkage to fixed support of the chain plate. $P_1 = 8mm$ is pitch of the chain, $\triangle T = 290K$ is temperature difference, $\alpha = 9 \times 10^{-6}/K$ is the coefficient of thermal expansion of titanium(Ti-5Al-2.5Sn ELI). X_{Max} and X_{Min} are maximum clearance and minimum clearance. ES and EI are the upper and lower deviation of holes. The es and ei are the upper and lower deviation of chain pin. The calculating results are show in TABLE 2.

TABLE 2. Calculating results

	Chain pin	Big hole	Small hole	Roller hole
Tolerances (mm)	$2^{\ 0}_{-0.01}$	$2^{+0.067}_{+0.072}$	$2^{-0.018}_{-0.004}$	$2^{-0.018}_{-0.004}$

2. *The simulation compared S chain with ordinary chain*

To evaluate the S-chain's low-temperature performance advantages over ordinary chains, we conducted comparative simulations analyzing stress distribution and deformation at 10K, 110K, and 210K. The results demonstrated the S-chain's superior cryogenic performance. For example, the stress of the S chain is less than the ordinary chain in the similar parts between two types of chains. The stress distributions of each component of the S chain at 10K are shown in Fig. 7, while the stress distributions of each component of the ordinary chain are shown in Fig. 8. The properties of simulating materials are shown at TABLE 3.

TABLE 3. Properties of simulated materials

	$\sigma_b(MPa)$	$\lambda\,(K^-1)$
Stainless steel	208	1.2×10^{-5}
Aluminum	280	2.3×10^{-5}
Titanium	930	9.4×10^{-6}

[a] Data taken from Ansys Workbench

The selected simulation models feature both types of chains with the same length. The middle link of each chain is chosen as the research object. Initially,, stainless steel was set as the material for chains and their stress are compared. Subsequently, the other simulation of chain are conducted to compare the stress of different material in the same temperature for selecting the best material. A significant disparity in stress exists between the two chain links. The maximum stress on the pin of the S chain is merely 2.63 MPa, whereas that on the pin of the ordinary chain reaches 25.71 MPa, nearly a tenfold difference. For the rollers and sleeves, the maximum stress difference between the two is about 84 MPa. It is evident that the stress on the roller and pin of the S chain is minimal and evenly distributed.

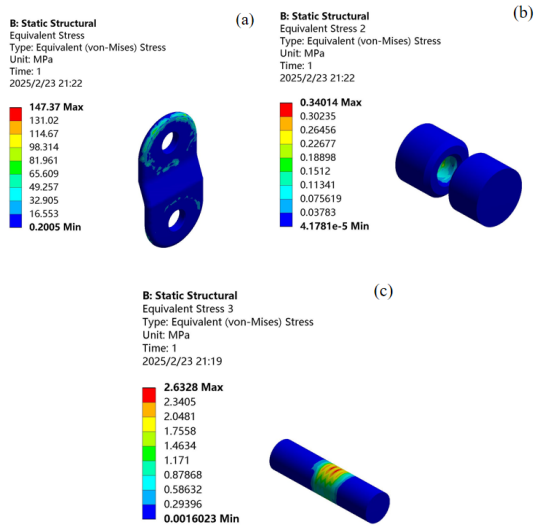

Fig. 7. Stress distribution of S chain part. (a) S chain plate; (b) S chain roller; (c) S chain pin.

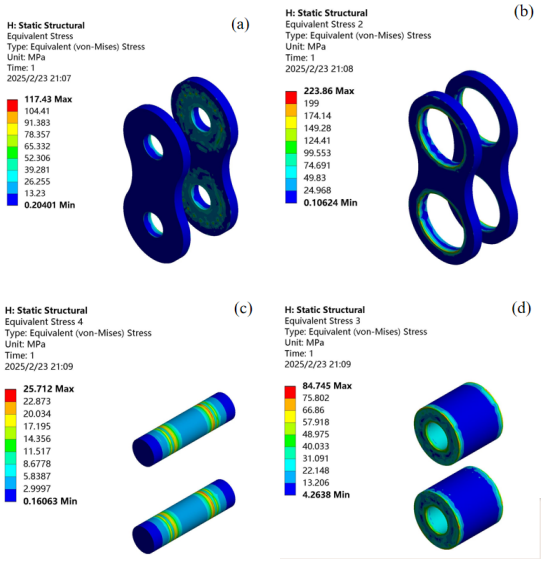

Fig. 8. Stress distribution of ordinary chain part. (a) Outer plates; (b) Inner plates; (c) Pins; (d) sleeves.

The maximum stress of outer plate is smaller than S chain plate, but the maximum stress distributed in S chain plate is not a critical position (sporadically distributed and located at the edges). The maximum stress of inner plate is 76 MPa higher than S chain plate and that is close to the yield strength of stainless steel. This phenomenon further explains why ordinary chain plates will bend and plastically deform after low-temperature testing.

The chain plate is the most important part in S chain, so some relevant simulations were conducted. Rays are drawn from the center hole of the outer and S chain plates at 0°, 90°, 180°, and 270°, respectively, as shown in Fig. 9. The stress

data on each ray 0-3 mm from the center hole is shown in Fig. 10.

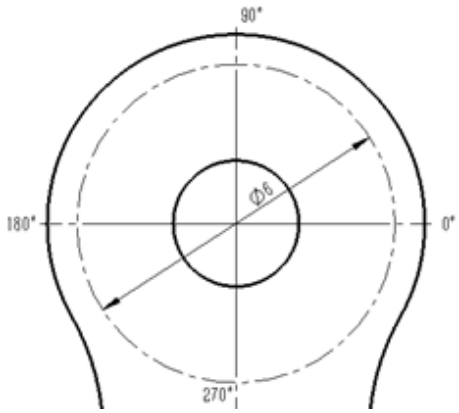

Fig. 9. Ray from central

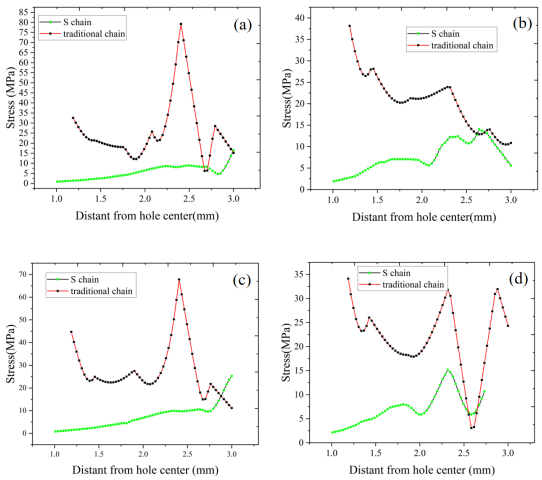

Fig. 10. Stress distribution at 10K (a) 0°; (b) 90°; (c) 180°; (d) 270°.

Only in the range 2.55 - 2.6 mm away from the hole center or at the end of the chain plate is the stress of the S chain plate slightly higher than that of the outer plate. In other positions, the stress of S chain plate is less than the outer plate. When comparing the rates of change, it becomes evident that the S chain exhibits a very gradual rate of change at 0° and 180°. Meanwhile, although the rate of change at 90° and 270° becomes somewhat steeper, it remains significantly gentler than that of the ordinary chain. The mentioned above implied the S chain is a great design and the S chain has higher fatigue limits and the S chain driver can work at lower temperature.

The Fig. 10(a) and Fig. 10(c) has a large peak in near to the distance from center of the plate hole 2.4mm and the diameter of inner plate hole is 4.9mm. This peak is effected by the edge of inner plate. The Fig. 10(d) has a deep valley is because far and far away the edge of inner plate. The stress increases again because the main deformation occurs at both ends of the outer plate.

The stress of plates is less than 10K under two other conditions. In addition, the stress distribution is similar to that of 10K. The S chain plate at 0° and the outer plate at 270° are employed to illustrate this conclusion in Fig. 11. This result shows that the stress distribution of both chains is similar under various temperature conditions. This finding provided much convenience for subsequent data processing and analysis.

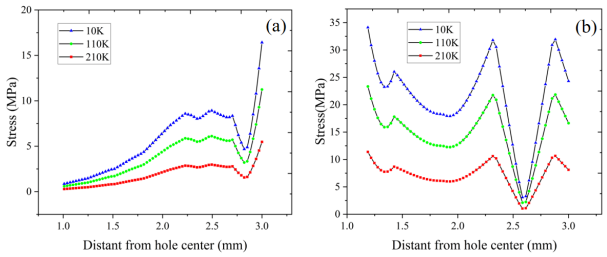

Fig. 11. Similar distribution of stress. (a) Stress distribute in different temperature of S chain plate; (b) Stress distribute in different temperature of ordinary chain plate.

In the direction perpendicular (Z-axis) to the chain plate, the shrinkage of the S chain plate is significantly less than that of the ordinary chain. The ordinary chain plates are symmetrically distributed in the XY plane and the inner surface of S chain is in the XY plane. Blue represents the deformation of the chain plates in the negative direction of the Z-axis, and red represents the deformation of the chain plates in the positive direction of the Z-axis. The simulating result is shown in Fig. 12. The deformation mainly occurs on both sides with less deformation on the inner side, whether it is the S chain plate or the ordinary chain plate. The deformation of the two is five times different and the inner plate will interact with the outer plate. This is why the ordinary chain will move to two side while low temperature testing. The S chain plate has very little impact on the next chain plate unlike ordinary chains. Therefore, the S chain plate is less likely to deviate left and right as mentioned above. This design may solve or reduce the above problems. The generation of tensile stress and the phenomenon of jamming will correspondingly decrease.

After simulating and comparing the material of stainless steel, different materials of chains were also compared at 10K. Some commonly used materials such as titanium (Ti-5Al-2.5Sn) and aluminum were selected. The simulation results are presented in Fig. 13. Aluminum exhibits superior performance compared to stainless steel and is more easily processed. However, its thermal expansion coefficient is excessively large, rendering it difficult to be utilized in low - temperature transmission. Metal materials typically exhibit reduced performance and are prone to low-temperature brittleness at low temperatures. The stainless steel chain had already undergone plastic deformation in previous tests. In order to ensure sufficient safety, aluminum alloys and stainless steal are also not suitable.

Although titanium is the most difficult to process, its performance at low temperatures is the best. Both the magnitude of stress and shrinkage are at their minimum. Finally, the tita-

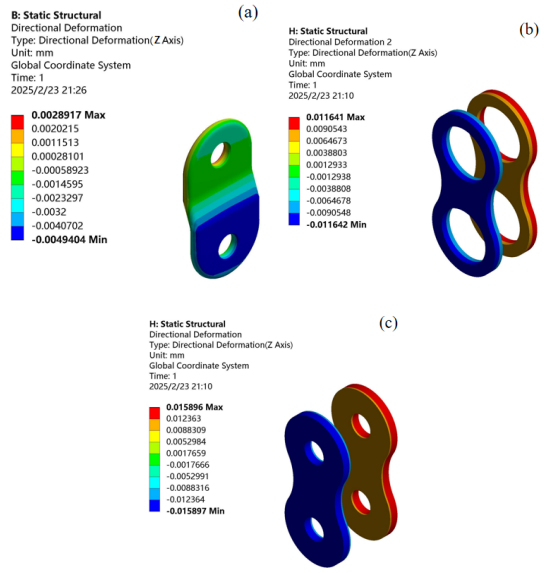

Fig. 12. Z-axis deformation simulation (a) S chain plate; (b) Inner plate; (c) Outer plate.

TABLE 4. Mechanical properties of Ti-5Al-2.5Sn ELI alloy

	20 °C			−253 °C	
Sample	σ_b/MPa	δ_5/%	α_{KU2}/kJ·m^{-2}	σ_b/MPa	δ_5/%
Impeller	805	15.5	620	1440	18
Wrought[a]	826	14.6	600	1460	17.6

[a] Data taken from Ref [43].

nium was selected for the S chain. The relevant performance parameters of titanium alloys are listed in TABLE 4.

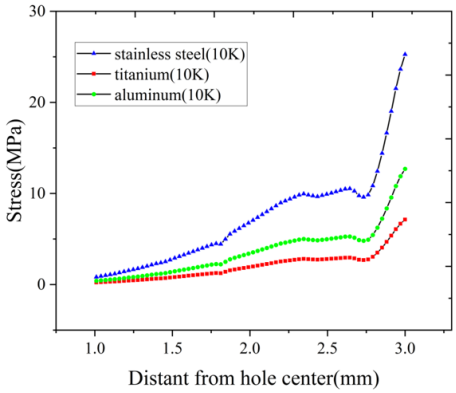

Fig. 13. Stress contribute of different material of S chain

The above shows that the S chain is more advantageous to operate under low temperature conditions. In order to ensure the normal operation of the chain, this paper also verifies the assumption of maximum displacement of the chain. The stress distribution of the S chain at various angles has been simulated, which provides a basis for selecting the optimal S chain. Two holes were set as fixed support to facilitate the research. The simulation results are shown in Fig. 14. Although the stress of the chain plate does not vary significantly with the angle as the clamping angle of the chain plate changes, the stress concentration at the corners of the chain plate becomes increasingly prominent. Therefore, the S chain plate with a clamping angle of 20° is finally selected. When the hole at one end of the chain plate is fixed, the deformation offset of the hole at the opposite end of the chain plate is shown in Fig. 14(f), with the maximum offset in the vertical direction measuring 0.023mm, a value similar to the calculated maximum offset of 0.022mm.

A full chain simulation was performed to enable a better comparison of the differences between the two chains. The results of the simulation and the data cloud are shown in Fig. 15. The stress distribution of the two chains has a clear regularity from Fig. 15(a). The rule is that the stress distribution patterns of the two chains are similar. As the temperature decreases, the stress gradually increases. The difference between the two types of chains can be clarified by studying the stress distribution at a distance of 80mm from the lowest temperature to high temperature. The stresses in the S chain are lower than the ordinary chain in most positions as can be seen in Fig. 15(b). The highest stresses in the S chain are located at the ends of the chain plates. In the case of ordinary chains, the maximum stress occurs in the middle of the chain plate. The difference in stress between the two is gradually apparent as the temperature decreases.

In the realm of simulation calculation, with the intention of simplifying the model and cutting down on the operation time, the coupling relationship between the S chain and the surrounding complex structure has been idealized. Consequently, it is impossible to achieve a comprehensive restoration of the entire actual engineering scene, which may lead to a certain degree of discrepancy between the simulation results and the real-world application. On the other hand, reducing the number of components also weakens the strength of the links.

B. Lower bracket

The lower bracket presents two issues: firstly, the shrinkage of the lower bracket is less than that of the chain, which will produce additional tensile stress. Secondly, the other one is the significant heat leakage to get a temperature lower than 10K. In order to improve the performance of the sample changer, the lower bracket has been newly designed.

The lower bracket is designed to be composed of two parts: a long support bracket and a low-temperature bearing support, as shown in Fig. 16. They are connected by welding. The long support bracket adopts a hollow design to reduce the difficulty of refrigeration and reduce the weight of the device.

In this simulation, the variation of the thermal conductivity of materials with temperature is taken into account. The thermal conductivity of stainless steel was obtained from Fluent's material database, while the thermal conductivity of titanium alloy was referenced from the research conducted by Mar-

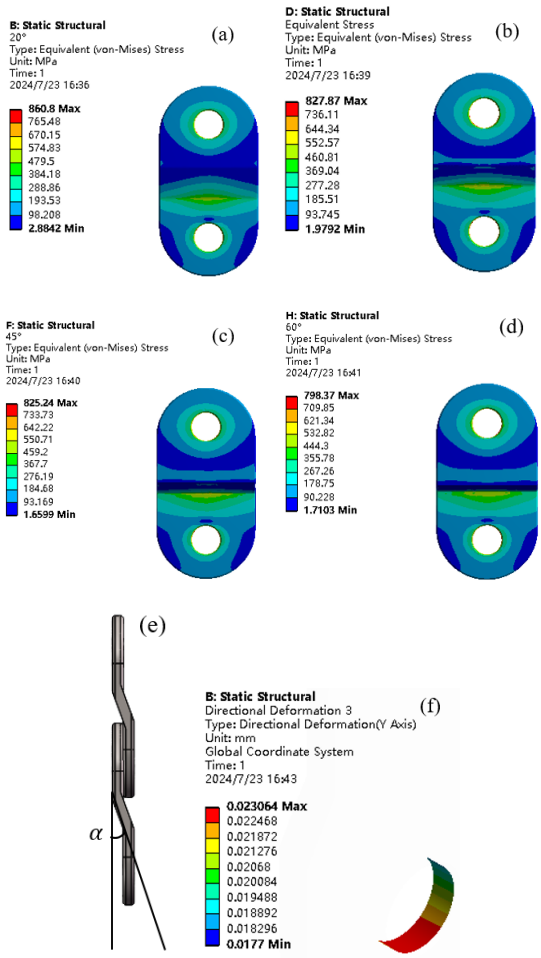

Fig. 14. Verification and angle simulated. (a) 20°; (b) 30°; (c) 45°; (d) 60°; (e) Chain plate angle; (f) Shrinkage of S chain plate.

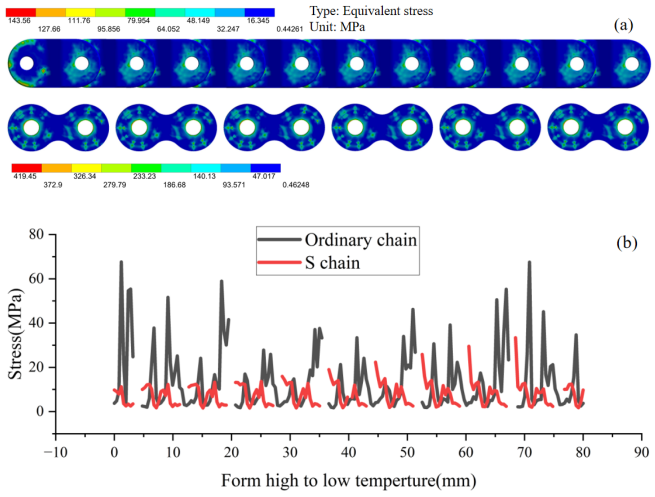

Fig. 15. Full chain simulation. (a) Stress distribute; (b) Compared of stress

quardt, E.D.[44]. In the simulation, both the 316 stainless steel solid structure and the 316 stainless steel hollow structure achieved a low temperature of 4.48K. The lowest temperature attained by the hollow titanium bracket was 4.23K. The temperature distributions of the three structures are presented in Fig. 17, showing similar temperature variations. The titanium alloy exhibits a longer low-temperature region with minimal temperature changes, a characteristic that can be advantageous for the precooling of samples.

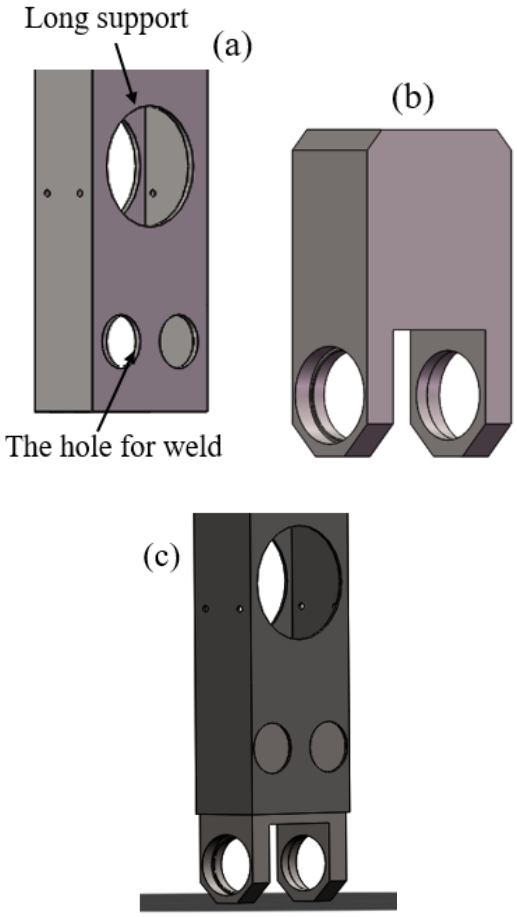

Fig. 16. Lower bracket. (a) Part of long support. (b) Cryogenic support; (c) Assemble model of lower bracket.

Titanium has the best performance under low-temperature condition. Our design requirement is a temperature range of 10K to 350K for the variation of the sample temperature. The design requirements can be met by the use of 316 stainless steel. Besides, the lager thermal expansion coefficient makes the shrinkage of lower bracket no longer less than the chain. That reduces the extra resistance for chain drive and solves the second problem mentioned above.

The detailed design of the S chain and the hollow structure of the bracket effectively solves the problem of chain jamming, running more smoothly and reducing friction. At the same time, it enables the sample to be cooled to below 10K, which also meets the design requirements.

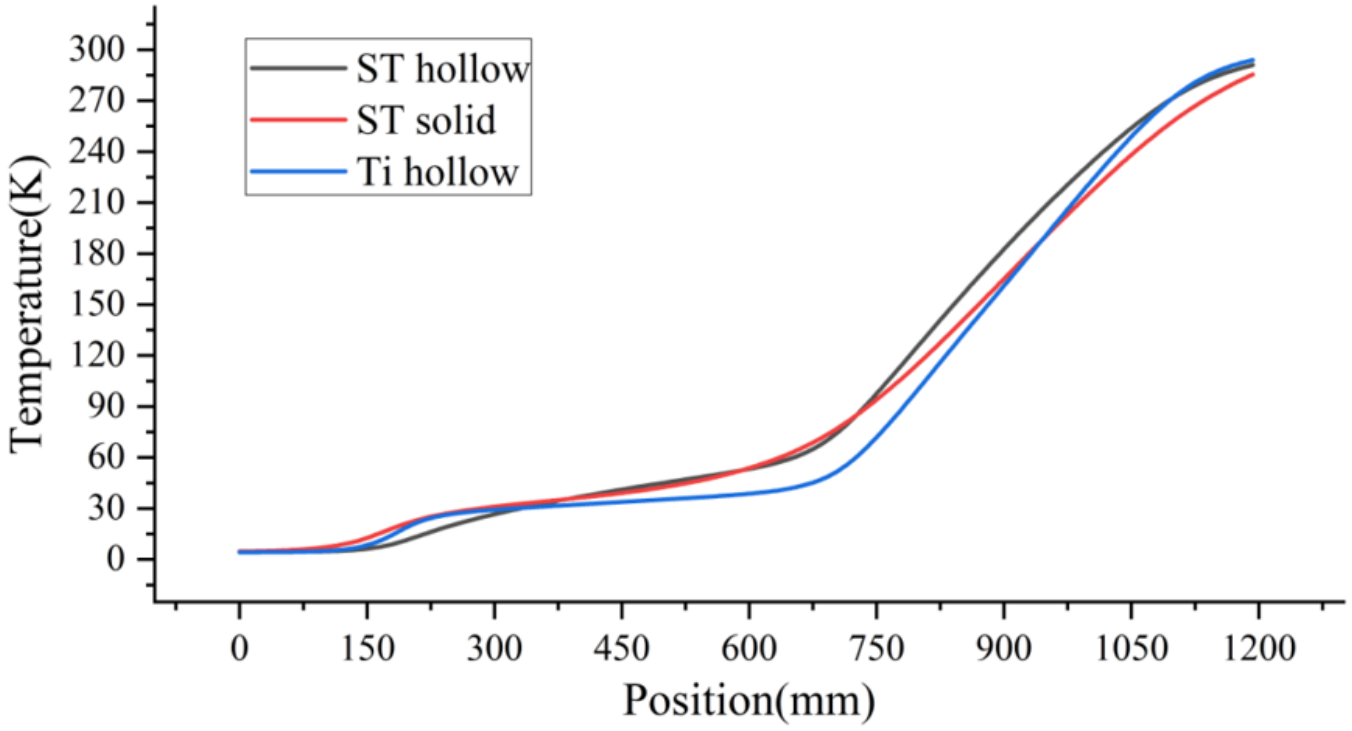

Fig. 17. Temperature distribute of three types of simulation

IV. CONCLUSION

CSNS has recently developed a cryogenic automatic sample changer that can operate in the temperature range of 100K-300K and finally exchange sample in 80K. After our testing, the measure point of the long bracket can take 6.6h to achieve 11K and keeps 10.83K final. This paper introduces the working principle of CCR-02 and the structure of the sample changer.

CSNS II phase will develop the automatic exchange technology in the temperature lower to 10K. Firstly, research was conducted to investigate why the chain drive jammed at 80K and an assumption of maximum displacement for the chain was proposed. Secondly, the chain and the structure of the support were redesigned. Finally, related simulations were conducted to explore its excellent performance.

The summary is as follows:

1) The CCR-02 can provide the temperature range of 4.2K-800K by a heater and the closed cycle refrigerator (CCR). Automatic sample changer for up to 24 samples under 80K, and keeps the lowest temperature at 10.83K. It takes within two minutes to exchange every sample.

2) The causes of the jamming phenomenon were thoroughly investigated, and a tentative assumption for the redesign process was proposed. Subsequently, an S chain was skillfully designed, and the lower bracket was strategically separated into two distinct parts.

3) Comparison of stress distribution and deformation of two chains at low temperatures using Workbench simulation. The maximum stress difference between the pin of two chains is about ten times (ordinary chain is higher than S chain). The maximum stress value of the inner chain plate exceeds the yield strength of stainless steel and the maximum stress difference between the roller and the sleeve is about 80 MPa. The stress distribution of the S chain is small and uniform.

4) Comparing the stress distribution of the two chain plates, the stress of the S chain is only slightly greater than that of the outer chain plate at 2.55-2.6 mm from the center of the hole. The stress distribution of the two chains under multiple temperature gradients is similar.

5) As the chain plate angle increases, the stress concentration phenomenon of the chain plate becomes increasingly obvious, and finally the S chain plate with a clamping angle of 20° is selected.

6) The lower bracket was redesigned to achieve better performance of the sample changer and finally can get the lowest temperature 4.23K and the sample can be well precooled when using titanium for the lower bracket. The long support frame is made of 316 stainless steel to solve the problem of extra pulling force and drive jamming.

The above is all the introduction about the low-temperature automatic sample changer. But there are still many tasks that need to be tested as the follows after the new automatic sample changer is processed:

1) Calibrate the sample temperature to facilitate rapid and accurate neutron scattering experiments.

2) Perform background tests on the cryogenic automatic sample changer.

3) Identify potential problems during the tests and carry out optimization.

[1] J. Wei, H.S. Chen, Y.W. Chen et al., China Spallation Neutron Source: Design, R&D, and outlook Nucl. Instrum. Methods Phys. Res. Sect. A. **600**, 10-13(2009). doi: 10.1016/j.nima.2008.11.017

[2] T. E. Mason, D. Abernathy, I, Anderson. et al., The Spallation Neutron Source in Oak Ridge: A powerful tool for materials research. Phys. B (Amsterdam, Neth.). **044618**, 955-960(2006). 10.1016/j.physb.2006.05.281

[3] F. Maekawa, M. Harada, K. Oikawa, et al., First neutron production utilizing J-PARC pulsed spallation neutron source JSNS and neutronic performance demonstrated. Nucl. Instrum. Methods Phys. Res. Sect. A.**620**, 159-165(2010). doi: 10.1016/j.nima.2010.04.020

[4] J.B. Yu, J.X. Chen, L. Kang. et al., Thermal analysis and tests of W/Cu brazing for primary collimator scraper in CSNS/RCS. Nucl. Sci. Technol. **28**, 46(2017) doi: 10.1007/s41365-017-0208-9

[5] J, Wu, X, Li, B. Wu. et al., Design and commissioning of a wideband RF system for CSNS-II rapid-cycling synchrotron. Nucl. Sci. Technol. **35**,5(2024). doi: 10.1007/s41365-024-01377-6

[6] L.H. He, S.H. Deng, F.R. Shen. et al., The performance of General Purpose Powder Diffractometer at CSNS. Nucl. Instrum. Methods Phys. Res. Sect. A. **1054**, 168414 (2023). doi: 10.1016/j.nima.2023.168414

[7] X.F. Jiang, J.R. Zhou, H. Luo. et al., A large area ^{3}He tube array detector with vacuum operation capacity for the SANS instrument at the CSNS. Nucl. Sci. Technol. **33**, 89 (2022). doi: 10.1007/s41365-022-01067-1

[8] J.R. Zhou, J.R. Zhou, Y.S. Song et al. Compact lithium-glass neutron beam monitor for SANS at CSNS. Nucl. Sci. Technol. **29**, 127 (2018). doi: 10.1007/s41365-018-0468-z

[9] L. Zhu, J.R. Zhou, Y.G. Xia. et al., Large area ^{3}He tube array detector with modular design for multi-physics instrument at CSNS. Nucl. Sci. Technol. **34**, 1 (2023). doi: 10.1007/s41365-022-01161-4

[10] I. Pivernifkova, M. Flugel, N. Paul, et al., Observation of preferential sputtering of Si/graphite anodes from Li-ion cells by GD-OES and its validation by neutron depth profiling. J. Power Sources **594**, 233972 (2024). doi: 10.1016/j.jpowsour.2023.233972

[11] Lee G H, N T D, Danielle Y, et al,. Magnetic Properties of the Ising-like Rare Earth Pyrosilicate: D-Er2Si2O7. Journal of physics. Condensed matter: an Institute of Physics journal **33**, 405801 (2021). doi: 10.1088/1361-648X/ac136a

[12] H.Y. Zhai, C.H. Liu, X.Q. Shang, et al., Measuring texture-component-dependent stress of CuZn39Pb2 by neutron diffraction. Int. J. Mech. Sci. 270, 109109 (2024). doi: 10.1016/j.ijmecsci.2024.109109

[13] S. Wang, H.T. Shi, D.X. Wang, et al., Neutron-based characterization: A rising star in illuminating rechargeable lithium metal batteries. Nano Energy, 122, 109337 (2024). doi: 10.1016/j.nanoen.2024.109337

[14] J. Chen, L.H. He, J.R. Zhang, et al., Planning of Energy-Selective Neutron Imaging Instrument at CSNS and its Application Prospect in Materials Science. Mater. Sci. Forum, 850, 161-166 (2016). doi: 10.4028/www.scientific.net/MSF.850.161

[15] Y. Li, P.J. Hou, R.R. Kamat, et al., Real-time evolution of texture and temperature during friction stir processing of a magnesium alloy: An operando neutron diffraction study. Acta Mater. 270, 119842 (2024). doi: 10.1016/j.actamat.2024.119842

[16] T. Hattori, K. Suzuki, T. Miyo, et al., Development of 0.5 mm gauge size radial collimators for high-pressure neutron diffraction experiments at PLANET in J-PARC. Methods Phys. Res. Sect. A. 1059, 168956 (2024). doi: 10.1016/j.nima.2023.168956

[17] H.B. Chen, R.Y. Li, Y. Liu, et al., Manufacturing and Testing of an In Situ Stretching Sample Environment Equipment for Neutron Scattering Experiments. Sci. Technol. Nucl. Install. 2020, 8867688 (2024). doi: 10.1155/2020/8867688

[18] A. Smith, B. Johnson, C. Brown, et al., Advances in neutron imaging at the NIST Center for Neutron Research. J. Appl. Phys. 123, 213901 (2018). doi: 10.1063/1.5020973

[19] X. Wang, Y. Zhang, Z. Li, et al., In situ neutron diffraction study of the phase transformation and thermal expansion behavior of a Ni-rich NiTiHf high-temperature shape memory alloy. J. Alloys Compd. 853, 157079 (2021). doi: 10.1016/j.jallcom.2020.157079

[20] R. Liu, J. Wang, Y. Chen, et al., In situ neutron diffraction study of the martensitic transformation and thermal expansion behavior in a Ni-rich NiTiHf high-temperature shape memory alloy. J. Alloys Compd. 852, 156984 (2021). doi: 10.1016/j.jallcom.2020.156984

[21] Z. Wu, Y. Sun, X. Zhang, et al., Investigation of the phase transformation and thermal expansion behavior of a Ni-rich NiTiHf high-temperature shape memory alloy by in situ neutron diffraction. J. Alloys Compd. 852, 156977 (2021). doi: 10.1016/j.jallcom.2020.156977

[22] L. Wang, H. Zhang, Z. Liu, et al., In situ neutron diffraction study of the phase transformation and thermal expansion behavior of a Ni-rich NiTiHf high-temperature shape memory alloy. J. Alloys Compd. 852, 156976 (2021). doi: 10.1016/j.jallcom.2020.156976

[23] Q. Zhu, S. Li, L. Xu, et al., In situ neutron diffraction study of the martensitic transformation and thermal expansion behavior in a Ni-rich NiTiHf high-temperature shape memory alloy. J. Alloys Compd. 852, 156962 (2021). doi: 10.1016/j.jallcom.2020.156962

[24] H. Chen, J. Zhang, S. Wang, et al., Development of a novel high-pressure cell for in situ neutron diffraction experiments at the China Spallation Neutron Source. Rev. Sci. Instrum. 91, 025101 (2020). doi: 10.1063/1.5142893

[25] S. Liu, X. Wang, L. Zhang, et al., In situ neutron diffraction study of the martensitic transformation and thermal expansion behavior in a Ni-rich NiTiHf high-temperature shape memory alloy. J. Alloys Compd. 852, 156967 (2021). doi: 10.1016/j.jallcom.2020.156967

[26] J. Wang, R. Liu, Y. Chen, et al., Investigation of the phase transformation and thermal expansion behavior of a Ni-rich NiTiHf high-temperature shape memory alloy by in situ neutron diffraction. J. Alloys Compd. 852, 156965 (2021). doi: 10.1016/j.jallcom.2020.156965

[27] Z. Sun, Y. Zhang, X. Li, et al., In situ neutron diffraction study of the phase transformation and thermal expansion behavior of a Ni-rich NiTiHf high-temperature shape memory alloy. J. Alloys Compd. 852, 156964 (2021). doi: 10.1016/j.jallcom.2020.156964

[28] L. Zhang, H. Wang, Z. Liu, et al., In situ neutron diffraction study of the martensitic transformation and thermal expansion behavior in a Ni-rich NiTiHf high-temperature shape memory alloy. J. Alloys Compd. 852, 156963 (2021). doi:

10.1016/j.jallcom.2020.156963
[29] Oak Ridge National Laboratory (Powder Diffractometer POWGEN — BL-11A — SNS). https://neutrons.ornl.gov/powgen/sample.
[30] A. Huq, M. Kirkham, P.F. Peterson, et al., POWGEN: rebuild of a third-generation powder diffractometer at the Spallation Neutron Source. Journal of applied crystallography, **52**, 1189-1201(2019). Doi: 10.1107/S160057671901121X
[31] Oak Ridge National Laboratory (Nanoscale-Ordered Materials DiffractometerNOMAD — BL-1B — SNS) https://neutrons.ornl.gov/nomad.
[32] ISIS Neutron and Muon Source (Iris Three Position Sample Changer 22 Sep 2016) https://www.isis.stfc.ac.uk/Pages/Iris-Three-Position-Sample-Changer.aspx Accessed 22 Sep 2016
[33] North, M., Kirichek, O., Burgess, G., et al. Current status of the ISIS robotic cryogenic sample changer. Journal of Neutron Research, **19**, 33-43 (2017). Doi: 10.3233/JNR-170049
[34] ISIS Neutron and Muon Source (Parachute Sample Changer 14 Sep 2016) https://www.isis.stfc.ac.uk/Pages/Parachute-Sample-Changer.aspx. Accessed 22 Sep 2016
[35] Japan Proton Accelerator Research Complex (Sample Environment (SE) at BL21) http://j-parc.jp/researcher/MatLife/en/se/bl21.html#bl21as01.
[36] H.T. Hu, M.J. Dou, C.C. Chun, et al., Development of an automatic sample changer with variable temperature for small-angle neutron scattering at China Spallation Neutron Source. *J. Appl. Crystallogr.* **52**, 1189-1201 (2019). Doi: 10.1063/5.0138705
[37] M.J. Dou, H.T. Hu, Z.Q. Zhang, et al., Development of a 10 K automated sample exchange cryostat for SANS_CSNS. *Cryogenics* **141**, 103881 (2024). Doi: 10.1016/J.CRYOGENICS.2024.103881
[38] X.Z. Zhang, M.F. Xu, Z.L. Chen, et al., Development of a superconducting undulator cryostat based on the thermosiphon effect. *Int. J. Refrig.* **164**, 86-94 (2024). Doi: 10.1016/j.ijrefrig.2024.05.009
[39] S.Q. Liu, Y.A. Song, H.Y. Zhang, et al., Achieving high stability in Cryostat: A study on optimal thermal link parameters. *Int. J. Refrig.* **167**, 13-22 (2024). Doi: 10.1016/j.ijrefrig.2024.07.026
[40] X.Z. Zhang, M.F. Xu, Z.L. Chen, et al., Thermal performance research on the zero liquid helium consumption cryostat for a superconducting undulator. *Energy* **308**, 132868 (2024). Doi: 10.1016/j.energy.2024.132868
[41] C.C. He, B. Ye, N. Li, et al., Development of Commissioning and operation of CSNS Cryogenic System. *IOP Conf. Ser.: Mater. Sci. Eng* **502**, 012017 (2019). Doi: 10.1088/1757-899X/502/1/012017
[42] S.Y. Zhang, H.T. Hu, B. Yuan, et al., Sample environment at the China spallation neutron source. *J. Neutron Res.* **21**, 7-15 (2019). Doi: 10.3233/JNR-180083
[43] Z.C. Lu, X.H. Zhang, W. J et al., Investigation on the deformation mechanism of Ti–5Al-2.5Sn ELI titanium alloy at cryogenic and room temperatures. *Mater. Sci. Eng* **818**, 141380(2021). Doi: 10.1016/j.msea.2021.141380
[44] Marquardt, E.D., Le, J.P., Radebaugh, R., Cryogenic material properties database. *Cryocoolers 11*, (2002). Doi: 10.3233/JNR-180083